ISSN (Print) 1226-1750
ISSN (Online) 2233-6656
Journal of Magnetics 24(2), 350-354 (2019) https://doi.org/10.4283/JMAG.2019.24.2.350

Orthogonality Correction for Concentric Tri-axis Fluxgate Magnetometer

Xuan Thang Trinh[1,5], Jen-Tzong Jeng[1]*, Chih-Cheng Lu[2]*, and Van Su Luong[3,4]

[1]*Department of Mechanical Engineering, National Kaohsiung University Science and Technology, Kaohsiung 80778, Taiwan*
[2]*Graduate Institute of Mechatronics Engineering, National Taipei University of Technology, Taipei 10608, Taiwan*
[3]*Faculty of Electrical and Electronic Engineering, Phenikaa Institute for Advanced Study (PIAS), Phenikaa University, Hanoi 100000, Viet Nam*
[4]*Phenikaa Research and Technology Institute (PRATI), A&A Green Phoenix Group, 167 Hoang Ngan, Hanoi 100000, Viet Nam*
[5]*Faculty of Mechanical Engineering, Hung Yen University of Technology and Education, Hung Yen 160000, Viet Nam*

(Received 15 July 2018, Received in final form 20 April 2019, Accepted 10 May 2019)

In this work, a compact tri-axis fluxgate magnetometer comprising a single magnetic core was implemented and the effectiveness of the orthogonality correction algorithm was demonstrated. The vector magnetometer consists of a tube-shaped soft magnetic flux chopper with a toroidal coil and three concentric pick-up coils. The tube-shaped flux chopper with magnet wires has the total dimension of 10 mm × 10 mm. The number of turns of the pick-up coils *X*-, *Y*-, and *Z*- are 110, 110 and 150, respectively. The center of flux chopper is also the geometric center of the three pick-up coils, of which the sensing directions are aligned along the Cartesian axes. The concentric design ensures a single field point for the three sensing axes. When using the tri-axis fluxgate magnetometer as an electronic compass, the geomagnetic field components converted from the demodulated outputs of the sensing coils shows high accuracy by using the voltage-to-field transfer matrix. The proposed fluxgate system is suitable for applications related to high-accuracy static magnetic field measurement, e.g. geomagnetic field monitoring, electronic compass, and magnetic field mapping.

Keywords : tri-axis magnetometer, fluxgate, magnetic sensor, magnetic fields

1. Introduction

The tri-axis magnetometers have been introduced and widely applied in many industrial fields, such as geophysical prospecting, position control, and electronic compass [1]. Over the past two decades, there are many types of vector magnetometer developed and introduced. The popular kinds of magnetometer worth mentioning includes fluxgate [2-4], anisotropic magnetoresistance (AMR) [5-7], Hall effect [8], tunneling magnetoresistance (TMR) [9, 10] and giant magnetoresistance (GMR) [11-13] sensors. A widespread application of vector magnetometer is geomagnetic measurement, for which the fluxgate magnetometer plays an important role owing to its high sensitivity and low-noise in the detection of quasi-static weak magnetic fields [2, 3]. The conventional design of tri-axis magnetometer consists of three sensing elements [14, 15], which are not necessarily on the same field point. In addition, the fluxgates with concentric sensing and feedback coils are usually bulky [16]. In fact, for more demanding applications, e.g. position sensing, motion tracking, and high-resolution magnetic field mapping, it is important to have the same field point for the three orthogonal sensing axes, while keeping the overall size as small as possible. To build the tri-axis fluxgate magnetometer with three sensing elements on the same field point, the design with the concentric magnetic core(s) and sensing coils has been introduced [4, 17, 18]. The three sensing elements were aligned along orthogonal directions, but the non-orthogonality between the three sensing axes can't be completely eliminated in the fabrication process [17]. The remaining non-orthogonality may have resulted from multiple factors, e.g. geometric asymmetry, misalignment, and non-uniform magnetic properties of cores. Therefore, an orthogonality correction procedure is indispensable to calibrate the sensing directions of the magnetometer. Some orthogonality correction

*Corresponding authors: Jen-Tzong Jeng,
e-mail: jtjeng@nkust.edu.tw,
Chih-Cheng Lu, e-mail: cclu23@ntut.edu.tw

This paper was presented at the IcAUMS2018, Jeju, Korea, June 3-7, 2018.

methods were successfully applied for some kinds of three-dimensional sensors, e.g., fluxgate, GMR, or TMR [9, 12, 15].

In our last report, a compact three-axis magnetic sensor was designed and demonstrated by using the three TMR sensors aligned along three axes of the Cartesian coordinates system inside of a tube-shaped flux chopper [10]. The ac modulation method and the chopping technique were applied to enhance the sensitivity and reduce the noise of the sensing elements. The linear transformation calibration was used to correct the sensing directions of the magnetometer and define the angle error between the actual sensing directions and the Cartesian axes. In this work, a compact three-dimensional (3D) fluxgate magnetometer with a single tube-shaped flux chopper core and three concentric sensing coils is designed, implemented and demonstrated. The orthogonality correction process is applied to solve the non-orthogonality error between the sensing axes of 3D fluxgate.

2. Experimental Details

2.1. Configurations of 3D-fluxgate and measurement system

The vector magnetometer consists of a tube-shaped soft magnetic flux chopper with a toroidal coil and three concentric pick-up coils, as shown in Fig. 1(a). The design of 3D fluxgate magnetometer is similar to the one reported in [4]. The flux chopper tube was designed to be 10 mm in height and 10 mm in diameter. The chopper core was made from a single layer of cobalt-based amorphous ribbon, Metglas Magnetic Alloy 2714A, from Metglas Inc [19]. To fabricate the tube-shaped flux chopper, a rectangular soft-magnetic ribbon 10 mm in width and 31 mm in length was sealed with paper tape and wrapped by enameled copper wires. The rectangle core with coils is then bent into a tube shape to form a toroidal coil. This method has the advantage of being easier to fabricate a toroidal coil without the need to thread the wires through the tube hole. The *X*- and *Y*- pick-up coils were formed by wrapping 110 turns of enameled copper wires around a rectangular frame, while the 150-turns *Z*- pickup coil was wrapped on a tube-shaped paper frame. The flux chopper was inserted into the center of the three concentric pick-up coils, which were aligned as orthogonal as possible. The concentric design ensures a single field point for the three sensing axes. The operation principle is similar to the flux-chopped TMR magnetometer reported in our previous work [10], in which the three-axis magnetometer consists of a tube-shaped soft magnetic flux chopper, and three TMR sensors were mounted along three sensing

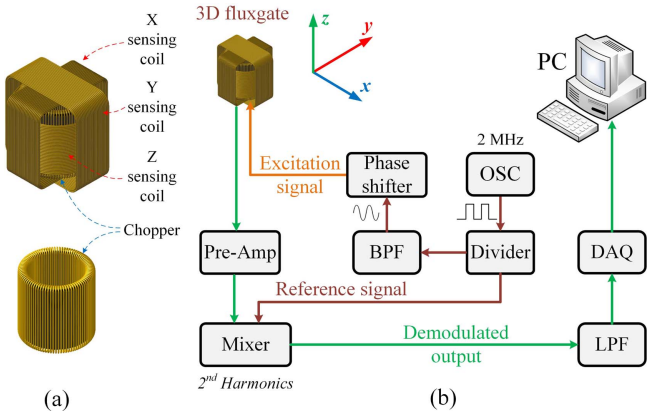

Fig. 1. (Color online) The configuration and driving system for the 3D fluxgate magnetometer.

directions.

By using the AC excitation signal to drive the chopper, the permeability of the sensor core is periodically saturated by the magnetization field, making the magnetization state of the soft magnetic material switch between saturated and unsaturated. The concentric sensing coils have better sensitivities at the higher frequencies and their outputs were demodulated at the second harmonics, which allows the magnetometer to be operated at frequencies above 1 kHz. The driving system for the 3D fluxgate sensor is shown in Fig. 1(b). The excitation signal is generated using a 2 MHz external crystal oscillator (OSC). To get a synchronized excitation signal, the frequency of square wave generated by OSC is divided by a counter IC (CD4040). The sine wave with a frequency of 31.25 kHz for the excitation signal is converted from the square wave with the same frequency by using a band-pass filter (BPF) before amplified by a power amplifier. The root-mean-square excitation current in flux chopper is about 80 mA. Each output of three sensing axes is amplified by an individual instrumentation amplifier (INA). Then the amplified output for each sensing axis is demodulated by a phase sensitive detector (PSD). To get the maximum the response of the demodulated output voltage, the phase of the excitation signal and the z-axis pick-up signal are tuned by analog phase shifters consisting of operational amplifiers AD811 from Analog Devices, Inc. A low-pass filter (LPF) was used to take the dc voltage component of modulated outputs, which represents the measured magnetic field. The sensitivity of 3D fluxgate was estimated by evaluating the slope of the voltage-field response. The noise was recorded via a Dynamic Signal Analyzer, SR780 from the Stanford Research Systems Inc. In order to minimize the interference from the environment, the sensor head was placed in a magnetic shielding chamber

during testing. A data acquisition (DAQ) device, model USB-6126 from the National Instruments, was used to implement the calibration process. Finally, the modulated outputs of the driving circuit are connected to the analog input of DAQ. The program for orthogonality correction algorithm was coded in LabVIEW software.

2.2. Orthogonality correction procedure

In the fabrication process, the three sensing coils are aligned in the directions so that their solenoid axes are orthogonal to each other. However, the non-orthogonality remains and is not negligible. The possible factors contribute to the non-orthogonality are alignment errors, geometric asymmetry of coils and cores, and the flux leakage at the closed-point gap of the toroidal core. In order to fix the non-orthogonality attributed by the remaining asymmetry in the chopper core and the misalignment in the sensor coils, the orthogonality correction algorithm was performed using a simple calibration process [12] to convert the sensor outputs into the orthogonal vector components of the geomagnetic field.

The Cartesian components B_x, B_y, and B_z of the external magnetic field are defined by the three sensing coils output voltage as the following equation:

$$\mathbf{B} = \begin{bmatrix} B_x \\ B_y \\ B_z \end{bmatrix} = \mathbf{AV} = \begin{bmatrix} A_{1x} & A_{2x} & A_{3x} \\ A_{1y} & A_{2y} & A_{3y} \\ A_{1z} & A_{2z} & A_{3z} \end{bmatrix} \begin{bmatrix} V_1 \\ V_2 \\ V_3 \end{bmatrix} \quad ,(1)$$

where A is the voltage-to-field transfer matrix with nine elements A_{ij} (i = 1, 2, or 3 and $j = x$, y, or z) and V is the matrix of sensing coils output. The symbols V_1, V_2, and V_3 denote the output voltage of X-, Y-, and Z-sensing coils, respectively. The elements of matrix A were determined by applying three reference magnetic fields, $B_{\text{ref-}x}$, $B_{\text{ref-}y}$, and $B_{\text{ref-}z}$, along three orthogonal directions. For calibrating the 3D-fluxgate, the three-axis orthogonal reference magnetic fields were applied by using a tri-axis Helmholtz coil, in which the 3D fluxgate was located at the center. The reference magnetic fields $B_{\text{ref-}x}$, $B_{\text{ref-}y}$, and $B_{\text{ref-}z}$ are the diagonal elements of matrix $\mathbf{B_{ref}}$, and the demodulated outputs of the three-sensing coils form the matrix $\mathbf{V_{cal}}$. The matrices $\mathbf{B_{ref}}$ and $\mathbf{V_{cal}}$ are defined as follows:

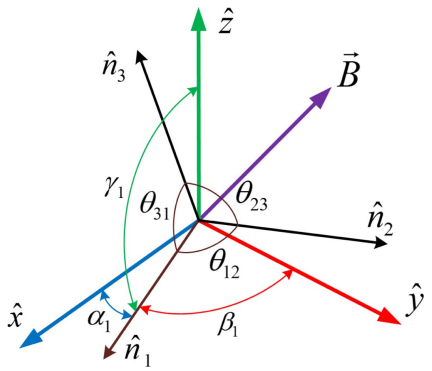

Fig. 2. (Color online) Spatial illustration for the unit vector and the actual sensing directions of 3D fluxgate magnetometer [10].

$$\mathbf{B_{ref}} = \begin{bmatrix} B_{\text{ref}-x} & 0 & 0 \\ 0 & B_{\text{ref}-y} & 0 \\ 0 & 0 & B_{\text{ref}-z} \end{bmatrix}, \text{ and} \quad (2)$$

$$\mathbf{V_{cal}} = \begin{bmatrix} V_{1x} & V_{1y} & V_{1z} \\ V_{2x} & V_{2y} & V_{2z} \\ V_{3x} & V_{3y} & V_{3z} \end{bmatrix} \quad (3)$$

Eqs. (1)-(3) indicate that the matrix $\mathbf{A}$ can be determined by $\mathbf{B_{ref}}$ and the inverse matrix of $\mathbf{V_{cal}}$ as follows [10]:

$$\mathbf{A} = \mathbf{B_{ref}}\,\mathbf{V_{cal}}^{-1} \quad (4)$$

When the matrix A is determined, the Cartesian components of an unknown magnetic field can be calculated from the output voltages of three sensing coils using (1). From (1), the effective sensitivities and sensing directions of three sensing coils can also be determined. The output of i-th sensing coil is a function of the sensitivity in the sensing direction along the unit vector $\hat{n}_i = \cos\alpha_i\hat{x} + \cos\beta_i\hat{y} + \cos\gamma_i\hat{z}$ as follows:

$$V_i = S_i\vec{B}\cdot\hat{n}_i = S_i(B_x\cos\alpha_i + B_y\cos\beta_i + B_z\cos\gamma_i) \quad (5)$$

Here the effective sensitivity $S_i = dV/dB$ corresponds to i-th sensing coil (i = 1, 2, or 3). The direction angles α_i, β_i, and γ_i are made between unit vector $\hat{n}_i$ and Cartesian x-, y-, and z-axes, respectively, as shown in Fig. 2. By comparison of (1) and (5), it can be seen that the elements of inverse matrix $\mathbf{A^{-1}}$ are the product of the effective sensitivities and the direction cosines of α_i, β_i and γ_i, as the following relation [10]:

$$\mathbf{A^{-1}} = \begin{bmatrix} S_1\cos\alpha_1 & S_1\cos\beta_1 & S_1\cos\gamma_1 \\ S_2\cos\alpha_2 & S_2\cos\beta_2 & S_2\cos\gamma_2 \\ S_3\cos\alpha_3 & S_3\cos\beta_3 & S_3\cos\gamma_3 \end{bmatrix} = \mathbf{M} \quad (6)$$

From (6), the angles θ_{12}, θ_{23}, θ_{31} between the actual sensing directions $\hat{n}_i$, $\hat{n}_2$ and $\hat{n}_3$ can be calculated from the elements of $\mathbf{A^{-1}}$ (or matrix $\mathbf{M}$). The orthogonality can be quantified by the deviation of θ_{12}, θ_{23}, θ_{31} from 90°.

3. Results and Discussion

3.1. Sensitivity and noise characterization

The sensitivities of 3D fluxgate were measured by applying the 0.125 Hz sweeping field along *x*-, *y*-, and *z*-sensing axes. The sensitivities were defined by the slopes of the *V*-*B* curve in the linear range with the root-mean-squared excitation current of 55 mA. The sensitivities of 3D fluxgate were found to be 3000 V/T, 2663 V/T, and 2434 V/T for *x*-, *y*-, and *z*-sensing axes, respectively. The minimum field noise levels are found to be 36, 52.5, and 43.2 pT/√Hz@1 Hz for *x*-, *y*-, and *z*- sensing axes, respectively. By employing the orthogonality correction method in [12] to solve the non-orthogonality errors, the matrix elements of matrix **M** were defined via an inverse matrix of *A*. The effective sensitivities and the actual sensing directions of the 3D fluxgate could be inversely calculated using the method in [10]. The performance comparison of fluxgate magnetometer before and after calibration is shown in Table 1. The effective sensitivities were found to be (S_1, S_2, S_3) = (2034.9 V/T, 1956 V/T, 2407 V/T). The direction angles of actual sensing axes $\hat{n}_i$, $\hat{n}_2$ and $\hat{n}_3$ are (α_1, β_1, γ_1) = (178.2°, 88.3°, 90.5°), (α_2, β_2, γ_2) = (88.68°, 178.3°, 91°), and (α_3, β_3, γ_3) = (90.3°, 92°, 2.02°), respectively. The angles formed between the actual sensing directions are (θ_{12}, θ_{23}, θ_{31}) = (93°, 90.2°, 89°). The result indicates that the maximum non-orthogonality of our 3D fluxgate was within 3° before calibration and 0.2° after calibration.

3.2. Azimuth response of calibrated magnetometer

The feasibility of the calibrated 3D fluxgate system for the electronic compass application was illustrated by rotating the magnetometer in the Earth's magnetic field. In this experiment, the tri-axis fluxgate sensor was attached on the manual rotation equipment rotating about the *z*-axis. The recorded azimuth responses before and after the calibration process are shown in Fig. 3. Fig. 3(a) and (b) illustrate the direct voltage output after demodulation, and Fig. 3(c) and (d) show the calibrated output of the vector magnetometer. The maximum responses to the *X*- and *Y*- components, as well as the averaged response to the Z-component, of the Earth's field are listed in Table 1 for comparison of un-calibrated and calibrated magnetometer.

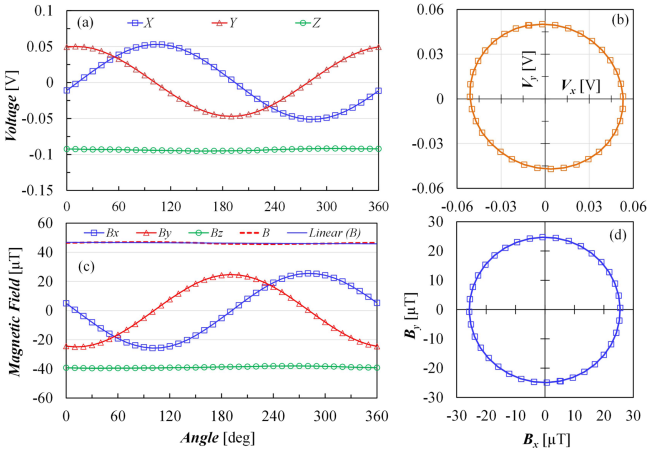

Fig. 3. (Color online) Azimuth response of 3-D fluxgate sensor. (a) Direct outputs of the sensing coils with rotating about *z*-axis (b) Polar plot of X-Y sensing coils outputs voltage (c) Calibrated magnetometer output after calibration (d) Polar plot of measured magnetic field component B_x and B_y.

The response to the Earth's field was recorded at the defined angles with the magnetometer rotating about the *z*-axis with 10° steps over the 360° range. Before recording the azimuth response in the Earth magnetic field, the DC offset component was removed electronically via the phase sensitive detection circuit. Fig. 3(a) shows the azimuth responses of the direct output voltage when the 3D fluxgate sensor was rotated about the *z*-axis. The Cartesian components of the geomagnetic field, which are converted from the direct outputs of the sensing coils by using the calibration algorithm, are shown in Fig. 3(c). The measured magnetic field shows that the azimuth response to B_x and B_y varies sinusoidally between +/−25 μT and 90° out of phase, while B_z is about constant at −39 μT. The measured magnetic field amplitude *B* is almost constant at 46 μT and independent of the rotating angles. The slight fluctuation of *B* may be caused by the non-uniform magnetic field from the passive and active devices nearby in the laboratory environment. The polar plot of demodulated outputs of *X*- and *Y*- sensing coils

Table 1. Performance comparison of 3D fluxgate before and after calibration.

Performance	Before calibration	After calibration
Sensitivities *X*/*Y*/*Z*	3000 V/T, 2663 V/T, 2434 V/T	2034.9 V/T, 1956 V/T, 2407 V/T
Maximum response to the *X*-component of Earth's field	0.0549 V	25 μT
Maximum response to the *Y*-component of Earth's field	0.05 V	25 μT
Averaged response to the *Z*-component of Earth's field	0.096 V	39 μT
Actual angle between *X* & *Y*	93°	90 ± 0.2°

was in a distorted shape, as shown in Fig. 3(b). The distortion in the polar plot is caused by the non-orthogonality as well as the dissimilar sensitivities of *X*- and *Y*-sensing axes. Fig. 3(d) indicates that the shape of polar plot becomes a circle centered at the origin (0,0) after the calibration process with offset correction [10]. Thus, the result indicates that the calibration processes described in (1)-(6) are useful to correct the non-orthogonality problem of the concentric 3D fluxgate to make the system behaves like a magnetometer having virtually orthogonal sensors. The proposed fabrication and calibration methods eliminate the requirement of a sophisticated adjustment process to align the three sensing axes mechanically with high accuracy.

4. Conclusion

The sensor design and orthogonality correction algorithm for a concentric 3D fluxgate magnetometer were presented and discussed. The effectiveness of orthogonality correction algorithm for a 3D concentric fluxgate sensor was verified successfully. The actual angles between the three axes to each other were found to be (93°, 90.2°, 89°) by using the data that retrieved from calibration algorithm. The maximum non-orthogonality of our 3D fluxgate was within 3° before calibration and reduced to be within 0.2° after calibration. The calibrated system shows substantial improvements in orthogonality of sensing axes and uniformity of sensitivities. The 3D concentric fluxgate magnetometer calibrated with the proposed orthogonality correction method is suitable for the applications related to high-accuracy static magnetic field measurement, e.g. geomagnetic field monitoring, electronic compass, and magnetic field mapping.

Acknowledgment

This work is supported by the Ministry of Science and Technology of Taiwan under Grant Nos. MOST 106-2221-E-151-025 and Grant MOST 106-2221-E-027-060.

References

[1] J. E. Lenz, Proc. IEEE. **78**, 973 (1990).
[2] F. Primdahl, J. Phys. E: Sci. Instrum. **12**, 241 (1979).
[3] P. Ripka, Sens. Actuators, A. **33**, 129 (1992).
[4] W. S. Watson, Single core triaxial flux-gate magnetometer. U.S. Patent No. 5,329,269, 12 Jul. 1994.
[5] P. Ripka, M. Vopálenský, A. Platil, M. Döscher, K.-M. Lenssen, and H. Hauser, J. Magn. Magn. Mater. **254**, 639 (2003).
[6] A. Platif, J. Kubik, M. Vopalensky, and P. Ripka, Precise AMR magnetometer for compass, Sensors, 2003. Proc. IEEE. 472, 2003.
[7] J. Včelák, P. Ripka, J. Kubik, A. Platil, and P. Kašpar, Sens. Actuators, A. **123**, 122 (2005).
[8] R. Racz, C. Schott, and S. Huber, Electronic compass sensor, Sensors, 2004. Proc. IEEE. 1446, 2004.
[9] V. S. Luong, J.-T. Jeng, J.-H. Hsu, C.-R. Chang, and C.-C. Lu, IEEE Trans. Magn. **52**, 4001204 (2016).
[10] V. S. Luong, J.-T. Jeng, C.-C. Lu, and H.-Y. Hsu, Meas. **109**, 297 (2017).
[11] J.-T. Jeng, C.-Y. Chiang, C.-H. Chang, and C.-C. Lu, IEEE Trans. Magn. **50**, 4000704 (2014).
[12] C.-Y. Chiang, J.-T. Jeng, B.-L. Lai, V. S. Luong, and C.-C. Lu, J. Appl. Phys. **117**, 17A321 (2015).
[13] X.-T. Trinh, J.-T. Jeng, C.-C. Lu, M.-J. Lan, B.-C. Chen, J.-H. Hsu, V.-S. Luong, and H.-Y. Hsu, IEEE Trans. Magn. **53**, 4004304 (2017).
[14] H. Joisten, B. Guilhamat, M. Audoin, J.-M. Leger, R. Cuchet, G. Barrois, J.-B. Albertini, P. Gaud, P. Renaux, and D. Bloch, IEEE Trans. Magn. **41**, 4356 (2005).
[15] K. Goleman and I. Sasada, IEEE Trans. Magn. **43**, 2379 (2007).
[16] F. Primdahl and P. A. Jensen, J. Phys. E: Sci. Instrum. **15**, 221 (1982).
[17] J. Kubík, J. Včelák, T. O'Donnell, and P. McCloskey, Sens. Actuators, A. **152**, 139 (2009).
[18] H. U. Auster, K. H. Glassmeier, W. Magnes, O. Aydogar, W. Baumjohann, D. Constantinescu, D. Fischer, K. H. Fornacon, E. Georgescu, P. Harvey, O. Hillenmaier, R. Kroth, M. Ludlam, Y. Narita, R. Nakamura, K. Okrafka, F. Plaschke, I. Richter, H. Schwarzl, B. Stoll, A. Valavanoglou, and M. Wiedemann, Space Sci. Rev. **141**, 235 (2008).
[19] Metglas 2714A Magnetic Alloy, Metglas Inc, accessed on June 26, 2018. [Online]. Available: http://www.metglas.com/products/magnetic_materials/2714a.asp.